Journal of Catalysis **195,** 113–124 (2000)
doi:10.1006/jcat.2000.2974, available online at http://www.idealibrary.com on IDEAL®

Oxidative Dehydrogenation of Butane over VMgO Catalysts

C. Téllez,* M. Abon,† J. A. Dalmon,† C. Mirodatos,† and J. Santamaría*,[1]

*Department of Chemical and Environmental Engineering, University of Zaragoza, 50009 Zaragoza, Spain; and †Institut des Recherches sur la Catalyse, 2 Avenue A. Einstein, Villeurbanne, France

Received March 20, 2000; revised June 16, 2000; accepted June 20, 2000

A VMgO catalyst has been characterized using a battery of both *in situ* and *ex situ* techniques in order to gain insight into the relationship between the state of the catalyst surface and the catalytic performance observed during the oxidative dehydrogenation of *n*-butane. It has been found that treating the catalyst under oxygen-rich or oxygen-lean atmospheres markedly changes the activity, selectivity, and rate of catalyst deactivation. The performance of the catalyst under both types of atmospheres is also notably different. A certain degree of catalyst reduction is desirable for this reaction, because it increases the selectivity to dehydrogenation products by limiting the amount of oxygen available at the catalyst surface. However, the performance of the catalyst under oxygen-depleted reaction atmospheres is not stable, the main cause for catalyst deactivation being the formation of coke. An overall analysis of the observed effects is proposed on the basis of a redox mechanism. © 2000 Academic Press

Key Words: **vanadium magnesia catalysts; oxidative dehydrogenation of butane; *in situ* characterization.**

INTRODUCTION

The oxidative dehydrogenation of butane (ODHB) is being intensely studied due to its potential advantages over conventional dehydrogenation: it is exothermic and therefore does not need an external heat input, avoids equilibrium limitations, runs at a lower temperature, and usually gives lower yields of coke and cracking products. ODHB has been carried out over a variety of catalysts that use mainly V (1–3) or Mo (4–6) on different supports. Among the best results reported to date, the VMgO system which contains mixed V and Mg oxides (7) was shown to be stable under continuous flow conditions, giving attractive selectivity to butene and butadiene (1, 2, 8). VMgO catalysts have also been successfully tested in other oxidative dehydrogenation reactions: propane (9–11), ethylbenzene (12–14), 2-methylpropane (15, 16), cyclohexane, (16), and 1-butene (12, 17). However, a poor selectivity was found for VMgO catalysts in the oxidative dehydrogenation of ethane.

[1] To whom correspondence should be addressed. Fax: +34 976 762142. E-mail: iqcatal@posta.unizar.es.

It is generally accepted that oxidative dehydrogenation on VMgO catalysts proceeds via the reduction of tetrahedrically coordinated V^{5+} ions, although the reduced state of the vanadium cations is still a matter of discussion (11, 18, 19). It seems also widely accepted that the initiation step of ODHB consists of the irreversible H abstraction on a secondary carbon to give a *sec*-butyl radical (1, 3, 20). A second hydrogen elimination leads to the alkene, which may desorb as such or undergo further transformation (to butadiene, CO, CO_2) on the catalyst surface. An acid/base balance is required, the acidity of the V^{5+} ions favoring the C–H attack and the basicity of surface oxygen (including the MgO support) favoring a rapid desorption of the olefins and diolefins, therefore reducing the probability of deep oxidation reactions (21). The orthovanadate phase was found to be more selective than the pyro- and metavanadate phases (1), although for the oxidative dehydrogenation of propane (ODHP) a better performance was reported for catalysts with a low V content, the active phase being an amorphous V overlayer (V^{5+} in isolated VO_4 units) supported over magnesia platelets (22–24).

Kung (2) with VMgO and Vrieland and Murchison (5) with Mo–Mg–O demonstrated that the reaction can take place in the absence of gaseous oxygen, using oxygen from the catalyst lattice. This enabled Soler *et al.* (26, 27) to carry out the reaction in a two-zone fluidized bed of VMgO catalyst. With this system the reaction takes place in the upper, oxygen-free zone of the bed and the catalyst is then recirculated to the oxygen-rich entrance region, where lattice oxygen is regenerated. The role of the gas-phase oxygen in ODHB seems to be limited to replenishing the spent lattice oxygen. In fact, as long as there is sufficient oxygen in the gas phase, there seems to be little or no influence of the oxygen partial pressure on the catalytic activity (apparent reaction order close to zero) (9). However, other authors report a certain influence of the oxygen partial pressure for V–Al–Mg–O (28) and V–Mg–O (29) catalyst, and a clearer dependence is demonstrated for the case of ODHP (24, 30).

Different mechanisms have been proposed to account for the observed kinetic behavior. Dejoz *et al.* (28) postulated a Langmuir–Hinshelwood model with dissociative and nondissociative adsorption to give dehydrogenation

0021-9517/00 $35.00

and deep oxidation products, respectively. In ODHP, Michaels *et al.* (31) and Stern and Grasselli (32) proposed a Mars–van Krevelen mechanism for dehydrogenation and a Langmuir–Hinshelwood mechanism for deep oxidation. Pantazidis (33), Jalibert (34), Schuurman *et al.* (25) and Téllez *et al.* (29) fitted their kinetic data using a dual-site Mars–van Krevelen mechanism in which different sites catalyze the formation of selective and nonselective oxidative dehydrogenation products. Boisdron *et al.* (35) and Zanthoff *et al.* (36) postulated the existence of different oxygen species in ODHP, namely O^{2-} and O^{-} for the production of propene and carbon oxides, respectively. Mamedov and Cortés-Corberán (37) proposed a Mars–van Krevelen model in which the selective reactions took place on partially reduced sites, while highly oxidized sites would yield deep oxidation products.

From the above, it seems that the redox behavior of the catalyst, in conjunction with factors such as cation reducibility and state of the catalyst under reaction conditions, is key to the catalytic performance during oxidative dehydrogenation of butane on V-based catalysts. It is therefore essential to follow the changes of the catalyst surface under reaction conditions in order to relate them to the observed catalytic performance. In this work a VMgO catalyst exposed to different reactive atmospheres has been thoroughly characterized in connection with its activity and selectivity for the ODHB reaction.

EXPERIMENTAL

Catalyst Preparation

An 8.5-g sample of MgO-supported vanadium oxide was prepared following a method described by Chaar *et al.* (1). MgO powder was impregnated with a solution containing 1 wt% of ammonium vanadate and 0.5 wt% of ammonium hydroxide. The resulting suspension was evaporated with stirring until a paste was obtained. This paste was dried at 120°C, and then calcined at 600°C, pelletized, crushed, and sieved to the desired particle size. The catalyst composition used in this work (termed VMgO catalyst in the remainder of this work) contained 24 wt% as V_2O_5.

Catalyst ex Situ Characterization

The fresh catalyst was characterized by BET measurements (Micromeritics, Pulse Chemisorb 2700) and by temperature-programmed reduction (TPR) experiments (Gow Mac Instruments). In TPR experiments a mass-flow-controlled stream containing 6% hydrogen in nitrogen was introduced over approximately 100 mg of catalyst contained in a quartz microreactor. The catalyst sample was then heated under a temperature ramp of 5°C/min.

The influence of the reacting atmosphere was studied by *ex situ* techniques on a previously equilibrated catalyst. Table 1 provides the different reaction conditions for the VMgO samples tested. In all cases, the reaction was carried out with 200 mg of VMgO catalyst in a quartz reactor at 500°C, under a butane partial pressure of 5 kPa. The samples were first heated to 500°C at 10°C/min under 200 Nml/min of He and the reacting gases were then introduced for 2 h at this temperature. After cooling of the samples under 400 Nml/min of He the catalyst was introduced in an He-inerted flask, sealed, and transported to the *ex situ* characterization equipment (NMR, ESR, XRD, XPS).

TABLE 1

Reaction Conditions Used with the Different VMgO Samples before Characterization

Sample	Molar ratio O_2/C_4H_{10}	Flow rate (ml/min)
Fresh	—	—
R05F2	0.5	200
R05F3	0.5	300
R10F2	1	200
R10F3	1	300
R20F2	2	200
R20F3	2	300

Note. In all cases, reaction took place at 500°C, with 200 mg of catalyst and under 5 kPa of butane in He. The oxygen concentration and the total feed flow rate changed for the different samples.

—Nuclear magnetic resonance of ^{51}V (^{51}V NMR) spectra were collected in a Bruker MSL-300 equipment, operating at 78.68 Hz under static or rotating conditions. The measurements were carried out at room temperature and referenced to $VOCl_3$.

—Electron spin resonance (ESR) measurements were carried out to compare the amount of bulk V^{4+} in the different samples. The data were collected at 77 K in a Varian E9 spectrometer, using a microwave frequency of 9.3 GHz. DPPH was used as a standard, with a gain of 2.0036.

—X-ray diffraction (XRD) analyses were carried out on a Phillips PW1710 difractometer using Ni-filtered Cu$K\alpha$ radiation and a graphite monochromator between 10–80° at a scan rate of 0.02°/s.

—X-ray photoelectron spectroscopy (XPS) data were acquired in a Shimadzu VG ESCA III model using Mg$K\alpha$ radiation, at a residual pressure of 10^{-8} Torr or lower. The C 1*s* line at 284.9 eV (corressponding to carbon impurities in the sample) was used as an internal standard. Atomic ratios were calculated using the area under the corresponding peaks, in conjunction with the Scofield cross sections, the mean free path of the electrons, and the instrument function, given by the manufacturer.

Catalyst in Situ Characterization

In situ diffuse reflectance Fourier transform infrared spectroscopy coupled to mass spectrometry (DRIFT-MS)

was used to characterize the adsorbed species on the catalyst surface under different reaction atmospheres. These experiments were carried out in a Spectra Tech catalytic cell adapted to a Nicolet 550 IR spectrometer and the outlet gases were analyzed continuously by on-line mass spectrometry (VG Instrument). About 20 mg of powdered catalyst sieved to 0.2–0.4 mm were heated in the DRIFT cell under Ar to the desired temperature. The typical operating sequence involved (i) stabilization of the catalyst under a 5/10/85 $C_4H_{10}/O_2/Ar$ mixture; (ii) purging with Ar; (iii) oxidation using a 4/4/92 O_2/He/Ar mixture; (iv) purging with Ar; (v) stabilization of the catalyst under a 5/2/93 $C_4H_{10}/O_2/Ar$ mixture; (vi) purging with Ar; and (vii) oxidation using a 4/4/92 O_2/He/Ar mixture.

Thermogravimetric (TG) experiments were carried out in a CI Electronics MK2 thermobalance. A 150-mg catalyst sample was loaded in a stainless steel wire mesh basket (125 μm openings) and heated under He to the desired temperature. The reacting mixture was then introduced. After ca. 6 h of reaction the reacting gases were switched off and the sample was cooled under He to 100°C. The reactor feed stream was then switched to a gas mixture containing 9% oxygen in He, and a temperature-programmed oxidation (TPO) of the catalyst was performed.

Reaction Experiments

Steady-state kinetic measurements were carried out on a 6-mm-internal diameter tubular quartz reactor inside an electrical furnace. The temperature was measured by a thermocouple inside a quartz well at the center of the catalyst bed which contained ca. 100 mg of VMgO catalyst. The reactor feed (200–400 Nml/min) contained premixed mass-flow-controlled streams (Brooks) of oxygen, butane, and He. The exit gases from the reactor were analyzed by on-line gas chromatography (HP 5890, with TCD and FID detectors, using Chromosorb PAW and Molecular Sieve 5A columns). Carbon balances were always better than ±5% and usually better than ±3% for the steady-state experiments reported in this work. Alternatively, transient reaction experiments were also performed in which the catalyst was brought to the reaction temperature under an inert feed and then a stepwise change in the feed concentration to either oxygen-rich or oxygen-lean feeds was effected. In this case the concentration of the different species at the exit of the microreactor was followed by mass spectrometry (Hiden HAL 2/201).

Anaerobic pulse experiments were performed by sending pulses containing a 1/1 butane/He mixture over the catalyst. The catalyst samples (40 mg) were first pretreated for 30 min under a given reaction atmosphere and pulses (ca. 1 ml) were then introduced by means of a six-way valve using a He (50 ml/min) carrier stream. Every outlet pulse was captured in a sample loop and analyzed by gas chromatography.

RESULTS

Catalyst Performance under ODHB Conditions

Figure 1 shows the changes in the selectivity to butadiene and the different butenes (*n*-butene, *cis*- and *trans*-2 butene) as a function of butane conversion (obtained by varying the space time under continuous flow) at 500 and 540°C, with different O_2/C_4H_{10} ratios in the feed. For a given conversion level, a higher selectivity to butadiene is obtained as the O_2/C_4H_{10} ratio decreases. However, while the production of butadiene is favored at low O_2/C_4H_{10} ratios (i.e., under oxygen-lean atmospheres), the selectivity to butenes is virtually unchanged: at a given temperature all the data points for different O_2/C_4H_{10} ratios fall on the same curve. The selectivity to CO and CO_2 (Fig. 2) follows the expected trend, being favored at high O_2/C_4H_{10} ratios. Figure 1 also shows that an increase in temperature not only increases the conversion as expected, but also, at isoconversion, both the butenes and butadience selectivity. This beneficial effect was also observed by Bhattacharya *et al.* (8) and by Blasco *et al.* (3). Finally, Fig. 1 also illustrates the well-known fact that butenes are primary products, with a high selectivity at low contact time (low conversion), while the secondary product butadiene appears at higher contact times.

Figure 3 shows the evolution of conversion and selectivity as a function of time. As the catalyst deactivates (decrease in

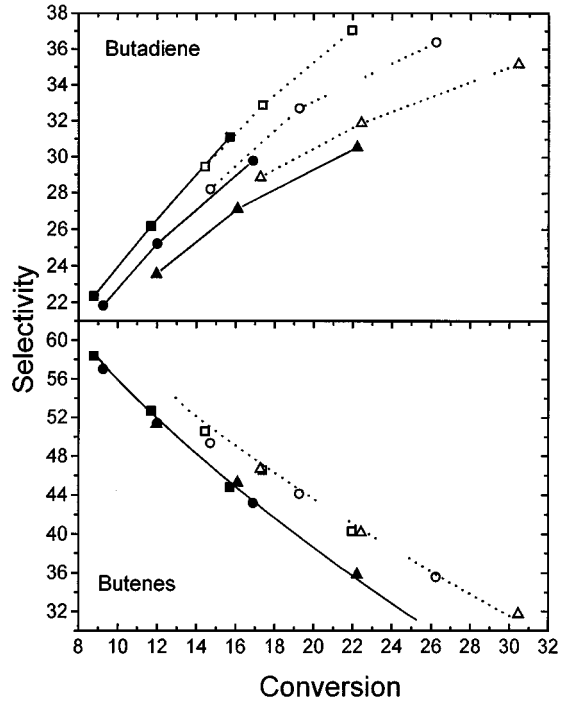

FIG. 1. Changes in the selectivity to butenes (1-butene, *cis*- + *trans*-2-butene) and butadiene with butane conversion; 100 mg of VMgO catalyst. Total flow rates: 200, 300, and 400 ml/min. Temperatures: 500°C (solid symbols) and 540°C (open symbols). Key: butane/oxygen/helium ratios 4/8/88 (▲, △), 4/4/96 (●, ○) and 4/2/92 (□, ■).

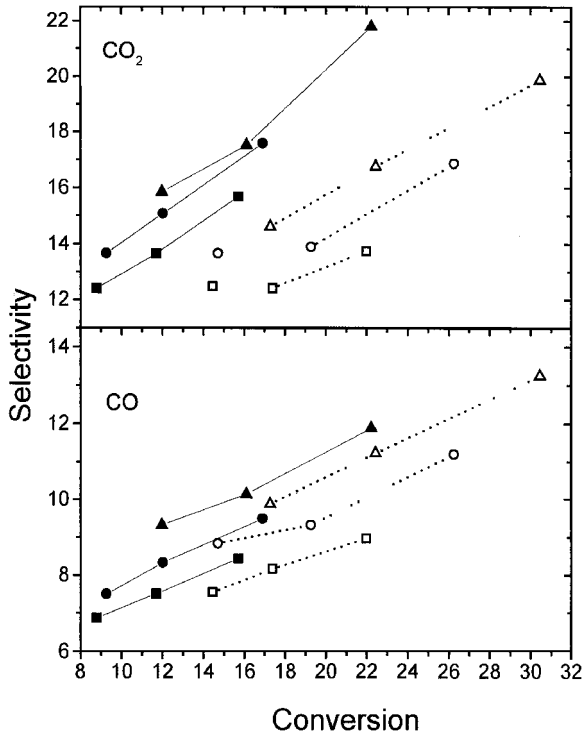

FIG. 2. Changes in selectivity to CO and CO_2 with butane conversion. Symbols as in Fig. 1.

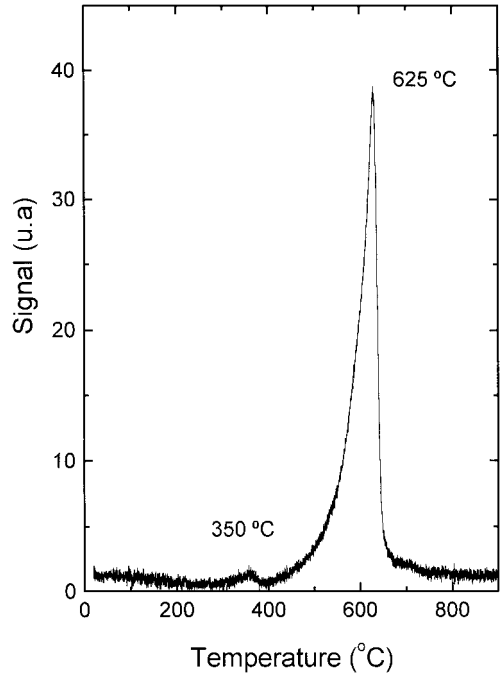

FIG. 4. TPR patterns of fresh V/MgO catalyst.

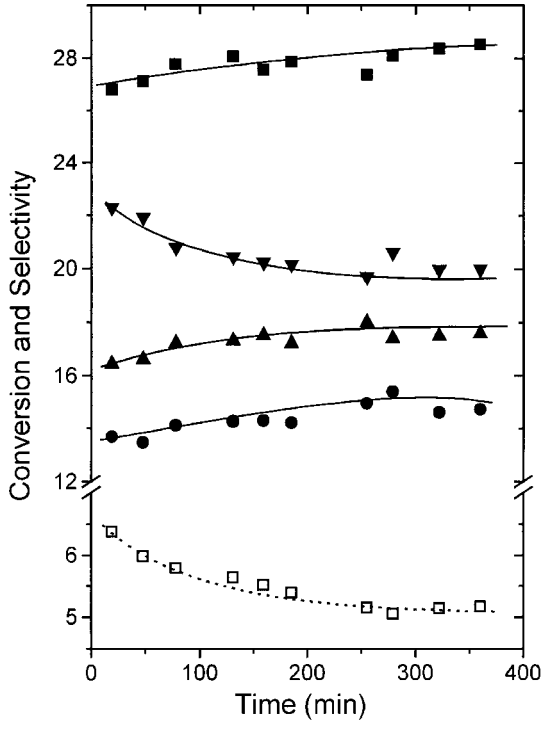

FIG. 3. Variation of the butane conversion (□) and of the selectivity to 1-butene (■), 2-*trans*-butene (●), 2-*cis*-butene (▲), and butadiene (▼) with time on stream at 500°C. C_4H_{10}/O_2/He ratio: 4/8/88. Total flow rate: 200 ml/min; 50 mg of VMgO catalyst.

butane conversion), the selectivity to butadiene decreases, while that to the different butene isomers increases. The decrease in catalytic activity appears to level off after ca. 4 h on stream, with the conversion still at about 75% of its initial level.

Characterization of Fresh and Used Catalysts by ex Situ Techniques

The fresh VMgO catalyst has a BET surface area slightly over 70 m^2/g and its performance was stable after 6 h of reaction at 500°C using a feed stream that contained 4% butane and 8% oxygen in He. As shown in Fig. 4, the main feature of the TPR pattern was a large peak at 625°C. A much smaller band at 350°C (between 320 and 410°C) was also present. According to Corma *et al.* (38) and Blasco *et al.* (3) the low-temperature peak can be assigned to the reduction of isolated V^{5+} species in distorted VO_4 units, while the high-temperature one would correspond to the reduction of V^{5+} belonging to bulk Mg orthovanadate ($Mg_3V_2O_8$). Recent XRD and EXAFS investigations carried out on similar VMgO catalysts indicated that under ODHP conditions either the isolated VO_4 units or the bulk orthovanadate were reduced into a spinel-like structure MgV_2O_4 (36, 39).

XRD experiments were carried out on the fresh catalyst and on samples R20F, R10F3, and R05F3 reacted under ODHB conditions with variable O_2/C_4H_{10} ratio (Table 1), from oxygen-rich (R20F3) to oxygen-lean (R05F3) atmosphere (Fig. 5 and Table 2). For all the samples the two main peaks observed at 43 and 62° correspond to MgO.

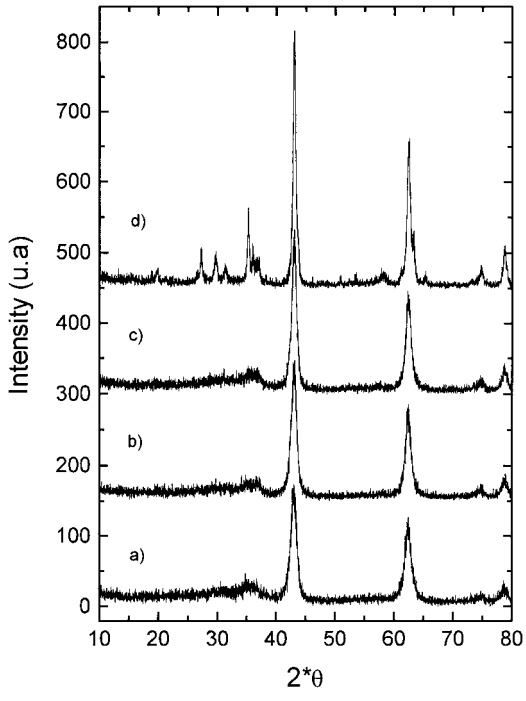

FIG. 5. XRD patterns of VMgO catalyst. (a) Fresh; (b) sample R05F3; (c) sample R10F3; and (d) sample R20F3 (see Table 1).

In addition, for sample R20F3 which was treated under the most oxidizing conditions, several small peaks indicating the presence of Mg orthovanadate ($Mg_3V_2O_8$) are evidenced; furthermore, neither pyro- ($Mg_2V_2O_7$) nor metavanadates (MgV_2O_6) are observed in this pattern. For the other samples treated under a lower oxygen concentration a diffuse band appears in the XRD patterns between 20 and 40° indicating a much less crystallized (or more dispersed) form of orthovanadate, and the same trend is observed for MgO crystals. The average MgO crystal size calculated from the XRD parameters (width over height ratio for the 43° band) increases from 7.8 (fresh catalyst) to 26.8 nm (R20F3); on the other hand, Mg orthovanadate was probably present as microcrystals in the oxygen-lean samples, and was clearly found as large crystals (50 nm) in the R20F3 sample.

The results of ^{51}V NMR experiments (not shown) under static conditions displayed a peak at 532–540 ppm and no signals in the 300 and 450 ppm region, which indicates the absence of nonselective species such as distorted octahedra ($Mg(VO)_3$) or square pyramids (V_2O_5). ^{51}V MAS NMR gave a single peak at 536–538 ppm, characteristic of orthovanadate (3, 40). This shows that Mg orthovanadate was present also in the samples where it could not be detected by XRD due to its small crystal size. Therefore both XRD and NMR measurements indicate a clear increase in crystallinity as the sample was treated under increasingly oxidizing conditions, the order being fresh catalyst < R05F3 < R10F3 < R20F3.

The surface atomic ratio determined from XPS analysis carried out on the fresh VMgO catalyst and on the used samples R05F2, R10F2, and R20F2 is reported in Table 3. For all the samples, the Mg/V ratio remained close to 7, i.e., far above the values expected from the $Mg_3V_2O_8$ orthovanadate phase (1.5) or the MgV_2O_4 spinel-like structure (0.5). In addition, the value obtained for the Mg/V atomic ratio was also higher than the value obtained by chemical analysis on the fresh sample (Mg/V = 6.66). The V $2p_{3/2}$ peak was deconvoluted into two bands, corresponding to V^{5+} and V^{4+} for higher and lower energies, respectively (41, 42). The V^{5+}/V^{4+} ratio was found to remain around 3 (i.e., ca. 75% of V^{5+}) for all the samples studied.

The fresh VMgO catalyst and the used R05F3, R10F3, and R20F3 samples were also examined by ESR, which is highly sensitive for bulk characterization. V^{4+} was clearly present in the fresh catalyst (not shown), with a spectrum typical of isolated V^{4+} in a distorted tetrahedron (40). In the sample treated with the lowest concentration of oxygen (R05F3) a significantly higher amount of V^{4+} was observed, as expected from the reduction effect already above mentioned. Although the absolute amount of V^{4+} cannot be quantified without a standard, the relative proportion in the different samples can be graded from the area corresponding to the V^{4+} peak. Thus, the amount of V^{4+} in the used

TABLE 2

XRD Results Obtained with Fresh and Used VMgO: Maximum Intensity (I_{Max}), Crystallization (I_{Max}/I_0), Background Intensity (I_{Back}), and Mean Diameter of MgO Crystal (D_{mean})

Sample	I_{max}	I_{Max}/I_0 (%)	I_{back}	D_{Mean} (nm)	Phases (other than MgO)
Fresh	163	46	14	7.8	Microcrystalline orthovanadate
R05F3	186	52	12	8.6	Microcrystalline orthovanadate
R10F3	221	62	12	11.0	Microcrystalline orthovanadate
R20F3	354 (I_0)	100	7	26.8	Orthovanadate

Note. The calculations were carried out using the peak at 43°C. I_0 represents the intensity of this peak in sample R20F3.

TABLE 3

XPS Results Obtained with Fresh and Used VMgO Samples

Sample	O_2/But	O_{1s} (eV)	$V_{2p3/2}$ (eV)	Mg_{2p} (eV)	Mg/O	V/O	Mg/V
Fresh		529.9	517.1	48.4	0.65	0.09	7.22
R05F2	0.5	530.7	517.9	49.5	0.76	0.11	7.00
R10F2	1	530.5	517.7	49.4	0.77	0.11	6.91
R20F2	2	530.3	517.4	49.2	0.78	0.11	6.96

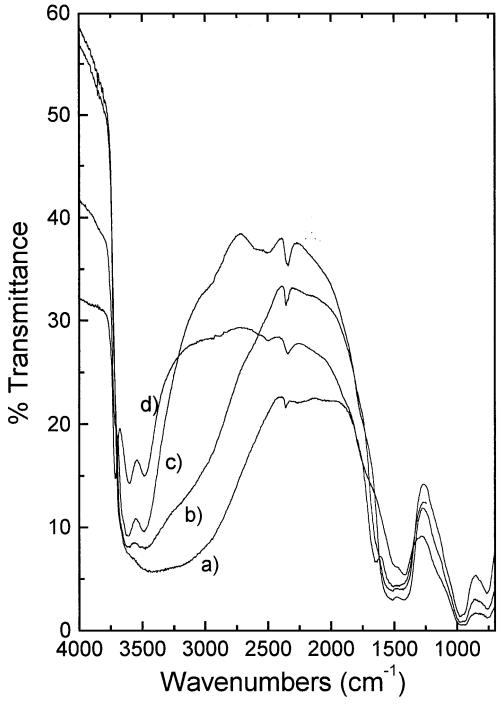

FIG. 6. Changes in the DRIFT spectra of the fresh VMgO catalyst upon heating under flowing Ar. (a) 23°C, (b) 160°C, (c) 360°C, and (d) 500°C.

samples is 1.78, 1.68, and 0.68 times that of the fresh catalyst for the R05F3; R10F3, and R20F3 samples, respectively. This confirms a clear increase in the V^{4+} content in parallel to the reducing character of the reaction atmosphere.

Catalyst Characterization under Reaction Conditions

Surface occupancy by in situ DRIFT spectroscopy. Figure 6 shows the evolution of the catalyst surface (DRIFT spectra) upon heating under an inert atmosphere (Ar) from room to reaction temperature (500°C). At room temperature, the fresh VMgO catalyst displays the bands at 960 and 730 cm^{-1} which are typical of Mg–O vibration in MgO and/or Mg vanadates (10, 38, 39). The presence of Mg carbonate/hydrogen carbonate is also revealed at 1400–1560 cm^{-1} (43), as expected from CO_2 adsorption over basic magnesium vanadate after calcination. The doublet band at 2300–2400 cm^{-1} indicates that gaseous CO_2 is being released from the surface (including possibly weakly adsorbed CO_2) and the absorption in the 3000–4000 cm^{-1} range includes both water (as also revealed by the band at 1640 cm^{-1}) and surface hydroxyl groups. Upon heating under Ar, water is slowly removed and –OH stretching bands become progressively evident. From 150°C acid OH^- groups can be identified, giving sharp bands at 3600 and 3480 cm^{-1} at 500°C. These bands also observed on pure V_2O_5 can be ascribed unambiguously to V–OH stretching vibrations. Basic hydroxyl groups at 3710–3700 cm^{-1} develop only above 400°C, being typical of MgOH abspecies (21, 44). This corresponds to a partial decarbonatation of the surface, as revealed by the simultaneous decrease of the carbonate bands in the 1400–1560 cm^{-1} range and the increased release of gaseous carbon dioxide. Note that a significant amount of magnesium carbonates remains at 500°C, as generally observed on magnesia-based catalysts (23, 41).

The DRIFT changes in surface coverage for different reaction atmospheres are best followed by subtraction of the corresponding spectra. To this end the catalyst was stabilized under argon flow at 500°C and then contacted with various reaction atmospheres. The results are reported in Fig. 7. Curves a and b respectively present the subtraction between the spectra corresponding to the catalyst equilibrated (15 min) under oxygen-rich (5/10/85 $C_4H_{10}/O_2/Ar$) and oxygen-lean (5/2/93 $C_4H_{10}/O_2/Ar$) conditions and that of the fresh catalyst stabilized under argon flow at 500°C.

After introduction of the oxygen-rich reaction mixture (5/10/85 $C_4H_{10}/O_2/Ar$) at 500°C (Fig. 7, curve a), bands at 1560–1600 and 1400–1450 cm^{-1} develop significantly. In agreement with Finocchio *et al.* (45), these bands could be ascribed to carboxylate species arising from the interaction of butene and/or butadiene with Mg vanadates. The presence of gaseous or adsorbed hydrocarbons is also revealed by the developing bands at 2800–3000 cm^{-1} which can be

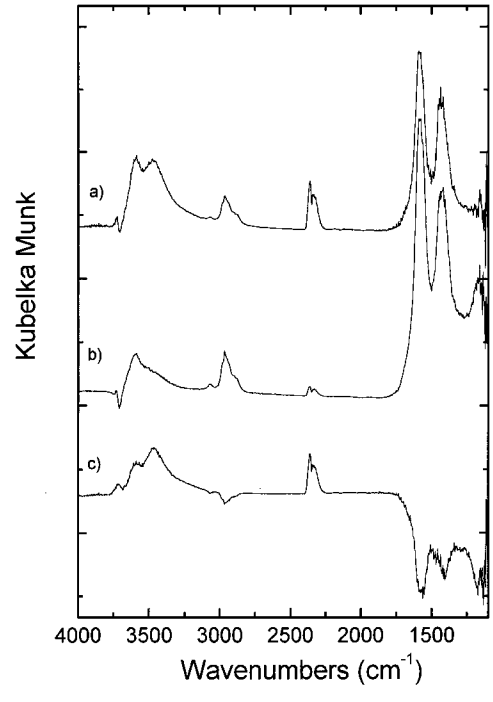

FIG. 7. Subtraction of DRIFT spectra recorded with the VMgO catalyst at 500°C. (a) 5 min under $C_4H_{10}/O_2/Ar$ ratio 5/10/85 minus fresh catalyst; (b) 5 min under $C_4H_{10}/O_2/Ar$ ratio 5/2/93 minus fresh catalyst; and (c) 5 min under $C_4H_{10}/O_2/Ar$ ratio 5/10/85 minus 5 min under $C_4H_{10}/O_2/Ar$ ratio 5/2/93.

attributed to aliphatic C–H, while the band at 3078 cm^{-1} is characteristic of C–H bonds in unsaturated hydrocarbons (43). On the other hand, similar results could also be assigned to adsorbed ethylenic M–CH=CH_2 adspecies, which gives IR absorption at 3100–2900, 1630–1565, and 1425–1385 cm^{-1}. Though the latter two are rather difficult to distinguish from the carboxylate bands in the spectrum, they could be ascribed to carbonaceous deposits possibly accumulating on the surface as coke precursors (via polymerization into polyaromatic intermediates, e.g., the so-called "coke peak," at ca. 1590 cm^{-1} (46)). A narrow band at 1200–1100 cm^{-1} could also tentatively be related to *sec*-butoxy- or alkoxy-type species (43). In addition, the reaction produces gaseous (or slightly adsorbed) CO_2 as can be seen from the increasing doublet at 2300–2400 cm^{-1}. The concentration of acidic OH^- groups (3480–3600 cm^{-1}) also increases markedly under oxygen-rich conditions, while there is almost no difference regarding the basic OH^-. This agrees with the findings of Pantazidis and Mirodatos (47) who reported that under ODHP conditions V–OH bonds are formed rather than Mg–OH.

When the reactive feed was replaced by Ar, transient recording of the IR spectra (not shown) indicated a fast disappearance of the bands corresponding to gas-phase CO_2 and C_4H_{10}, while the bands corresponding to the carboxylates/carbonaceous species decreased only slightly. The peak at 3078 cm^{-1} was still observed under Ar, which strengthens its attribution to carbonaceous species rather than to a gas-phase component. This statement was further confirmed by the disappearance of the 3078 cm^{-1} band after contacting again the catalyst with a O_2/Ar atmosphere. In a similar way, the peak at ca. 1590 cm^{-1} decreased under O_2/Ar, indicating the removal of oxidable carbonaceous species.

The subtraction of the spectra corresponding to the catalyst after introducing the oxygen-lean reaction mixture (5/2/93 C_4H_{10}/O_2/Ar) and the fresh catalyst (Fig. 7, curve b) shows a similar behavior, although the accumulation of the carbonaceous species at 3078 and 1590 cm^{-1} is more marked, as expected from a O_2/C_4H_{10} ratio which favors coke formation. When the oxygen-lean atmosphere was switched to O_2/Ar (not shown) both bands decreased, but were still observed (together with gaseous CO_2) after 15 min. Thus, a 15-min regeneration treatment at 500°C using a 4 vol% O_2/Ar mixture at 500°C was not sufficient for totally removing the carbonaceous deposits formed on the catalyst surface under oxygen-lean conditions.

Curve c in Fig. 7 which is obtained by subtracting curve (ii) from curve (i) summarizes the difference between rich and lean conditions: (i) more carbonaceous and/or carboxylate species are accumulated on the surface under oxygen-lean conditions, (ii) a larger concentration of hydroxyl groups (essentially acid) and of gaseous CO_2 develops under more oxidising conditions.

Dynamic Response of the Catalytic System to a Step Transient Switch from Inert to Reaction

DRIFT analysis. The dynamic change in the IR concentration of the above-described adspecies when switching from inert to a given reaction atmosphere was followed by recording DRIFT spectra every 5 s. Figure 8 reports these normalized changes determined from the integration of the corresponding IR bands (Gram Schmidt method). As can be seen, both basic (3710–3700 cm^{-1}) and acid (3480–3600 cm^{-1}) hydroxyl groups rapidly increase, reaching a maximum shortly after introduction of the reacting mixtures, followed by a small decrease to a stable level. Let us recall that the relative concentration of acid OH^- groups under oxygen-rich conditions was 2.5 times higher than that under oxygen-lean conditions. A similar dynamic behavior is observed for gaseous CO_2 under oxygen-rich conditions with a fast increase to a maximum (the catalyst is initially oxidized) and a small drop to a stable plateau. Under oxygen-lean conditions a maximum is also rapidly attained but the CO_2 concentration then decreases monotonically, indicating catalyst deactivation. Finally, the bands corresponding to C–H bonds (2800–3000 cm^{-1}), carboxylates/carbonaceous compounds (1590 cm^{-1}) and C=C carbonaceous species (3078 cm^{-1})

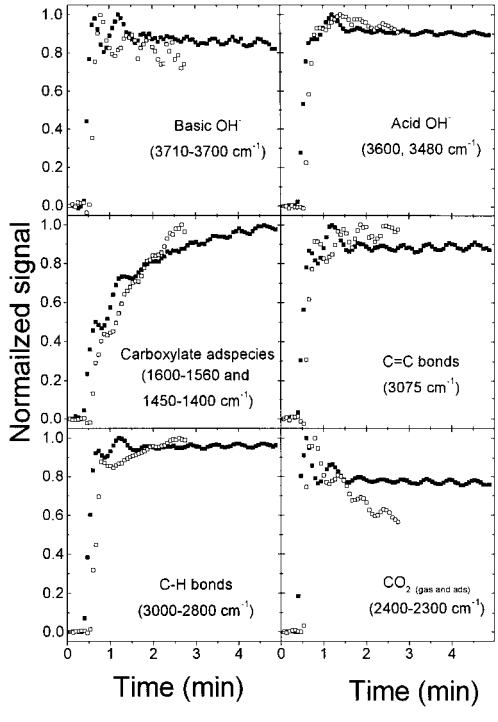

FIG. 8. Evolution of the normalized concentrations of several adsorbed and gaseous species over VMgO. The concentrations were obtained from characteristic bands in the DRIFT spectra, recorded as a function of time on stream after a feed switch from inert to oxygen-rich (10% O_2, ■) and oxygen-lean (2% O_2, □) reaction conditions respectively.

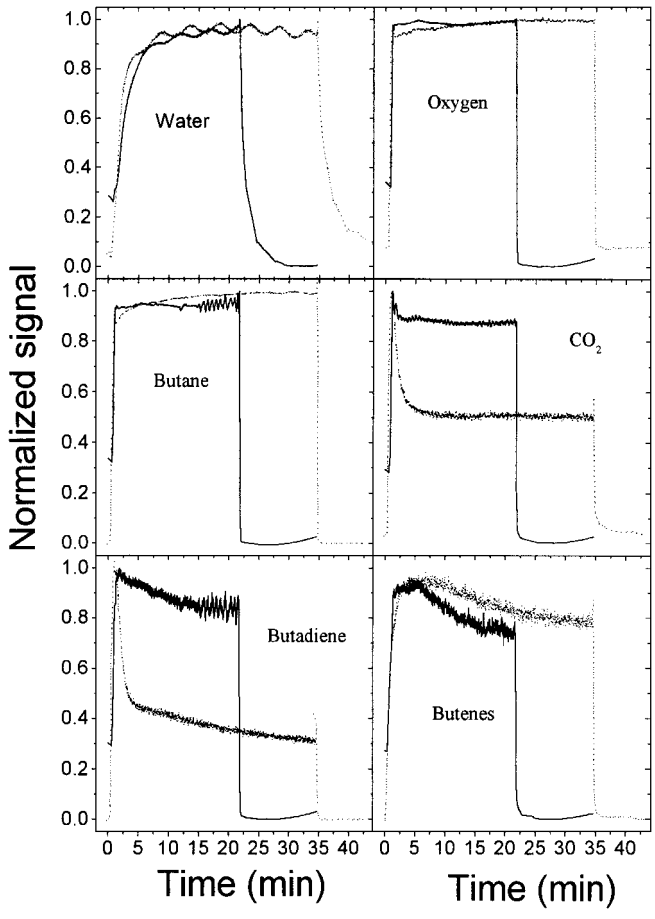

FIG. 9. Evolution of the normalized concentrations of different gaseous species at the reactor exit. The concentrations were obtained as a function of time from the corresponding mass spectrometer signals after a feed switch from insert to oxygen-rich (10% O_2, solid line) and oxygen-lean (2% O_2, dotted line) reaction conditions respectively.

increase with time for oxygen-lean conditions, while they either reach a stable level (C−H and C=C carbonaceous) or increase more slowly (carboxylates/carbonaceous compounds) under more oxidizing conditions. This again indicates a build-up of carbonaceous species when the catalytic surface is exposed to a higher hydrocarbon/oxygen ratio.

Gas-phase MS analysis. The transient evolution of the different species during the step switch from inert to reaction feed was followed by continuously monitoring the outlet gas stream by mass spectrometry. Figure 9 shows that water, oxygen, and butane follow similar normalized patterns, either under oxygen-lean or -rich conditions. However, the absolute level of each gas was different under both sets of conditions since the catalyst is less active under an oxygen-lean feed. Despite the similar normalized variation, a closer examination reveals that the butane and oxygen signals are relatively constant for the catalyst under the oxygen-rich atmosphere, while they slowly increase (i.e., the conversion decreases) under oxygen-lean conditions. Again, this clearly indicates that catalyst deactivation is taking place under oxygen-lean conditions. Another significant difference is observed for the responses of CO_2 and butadiene: under the oxygen-lean atmosphere a sharp maximum is observed in the production of these species before reaching a pseudo-steady-state level. This initial CO_2 and butadiene productivity could be related to a pool of active oxygen species available on the catalyst surface after exposure of the catalyst to the oxygen-rich mixture. As soon as the surface is reduced by the oxygen-lean reacting mixture, the production of CO_2 and butadiene stabilizes at a much lower level. It is however interesting to note that the formation of butenes does not present such an initial spike under an oxygen-lean atmosphere. In contrast, a smooth increase in the total production of butenes during the first few minutes on stream can be observed: as the catalyst is reduced the selectivity to butenes increases, and this effect initially compensates (in terms of yield to butenes) the drop in conversion due to the simultaneous catalyst deactivation. A similar trend was reported previously (Fig. 3).

Catalyst regeneration. When the catalysts treated under oxygen-rich and oxygen-lean atmospheres were regenerated under flowing oxygen at 500°C, the results (not shown) indicated a much larger production of CO_2 (3.3 times) and a correspondingly higher consumption of oxygen for the catalyst reacted under the oxygen-lean as compared to oxygen-rich atmosphere. This demonstrates an approximately 3-fold increase in coke build-up for the catalyst surface under oxygen-lean conditions.

Kinetics of Coke Deposition under Reaction Conditions Studied by Thermogravimetry

Figure 10 reports the change in VMgO catalyst weight measured in a thermobalance as a function of time. Initially (stage a), the sample loses over 7 wt% under the inert atmosphere which corresponds to the removal of water and surface carbonates, in agreement with DRIFT observations. After weight stabilization at 500°C an oxygen-lean feed containing 1.2% O_2 and 8% butane in He was introduced (stage b). It can be seen that the catalyst weight decreases rapidly and then increases again slowly. The first weight loss can be ascribed to the catalyst reduction by the oxygen-lean reaction mixture, a relatively fast process that dominates over the weight increase due to coke deposition. The latter eventually leads to a catalyst weight gain up to 2.8 wt% under oxygen-lean conditions, compared to a gain of only 0.13 wt% when an oxygen-rich (4% butane, 8% oxygen) reacting feed was used (not shown).

After purging and cooling down, the catalyst was again heated under an O_2/He stream (stage d). In this case the reverse effects of stage b were observed, i.e., an initial weight gain corresponding to catalyst reoxidation followed by a fast weight loss corresponding to the combustion of the

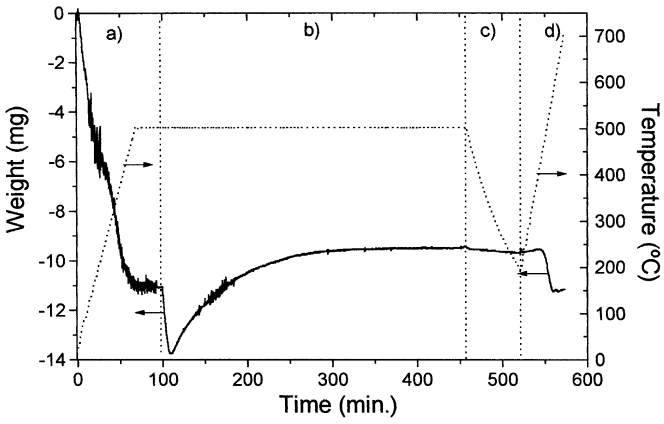

FIG. 10. Variation of catalyst weight (solid line) and temperature (dotted line) with time. Initial weight (fresh catalyst), 100 mg; total flow rate, 200 ml(STP)/min. Other operating conditions: (a) heating under helium; (b) reaction, $C_4H_{10}/O_2/He = 4/1.2/94.8$; (c) cooling under He; and (d) temperature-programmed oxidation, $O_2/He = 8/88$.

deposited coke, after which the initial weight of the catalyst (at the end of stage a) was approximately recovered.

The coke–time data gathered during stage b were fit to a simple potential model (48),

$$\frac{dC_c}{dt} = k(C_{c_{max}} - C_c)^n, \qquad [1]$$

where C_c represents the coke weight on the catalyst (grams of coke per gram of catalyst) and $C_{c_{max}}$ represents the maximum coke concentration attainable. A good fit was obtained ($R^2 = 0.999$ under oxygen-lean and $R^2 = 0.946$ under oxygen-rich conditions respectively) giving $n = 1.10$ (oxygen-lean) and $n = 0.984$ (oxygen-rich), which indicates that coke formation follows approximately a first-order deactivation rate with respect to coke (i.e., coke deactivates its own formation). Interestingly, the values of $C_{c_{max}}$ predicted by the model depended strongly on the operating conditions: 0.17 and 4.5 wt% of coke on the catalyst for oxygen-rich and oxygen-lean conditions, respectively.

Catalyst Behavior under Anaerobic Conditions

Figures 11 and 12 show the results of anaerobic experiments in which butane pulses were sent over a catalyst that had been previously equilibrated under a reaction atmosphere containing 5% butane and 8% oxygen in He. The first pulse gave a selectivity to butenes and butadiene of about 74%, which is close to the value obtained under continuous flow conditions. The selectivity to butenes and butadiene then increases for the next few pulses while the CO_x selectivity decreases, demonstrating as expected that the catalyst becomes more selective as it is reduced. From the fifth pulse onward the selectivity to butadiene starts

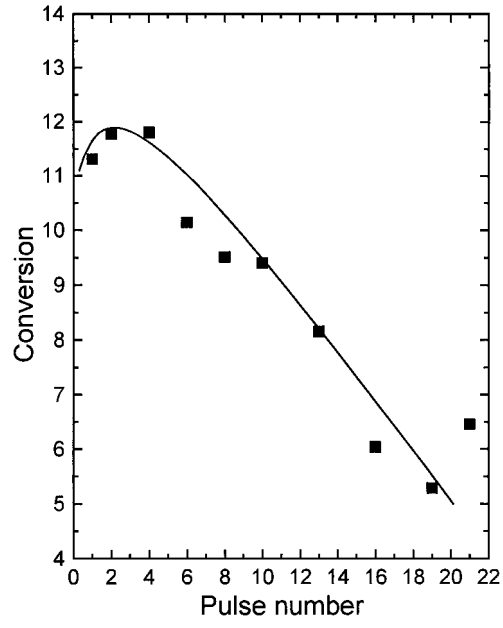

FIG. 11. Butane conversion in anaerobic experiments using anaerobic butane pulses. Before the pulses the catalyst was equilibrated under reaction atmosphere $C_4H_{10}/O_2/He = 4/8/88$. Catalyst weight, 40 mg; total flow rate, 300 ml/min; temperature, 500°C.

to decrease to the increase of the selectivity to butenes, while both the butane conversion and CO_x selectivity decrease continuosly. However, it must be noted that the decrease in butane conversion is approximately linear with

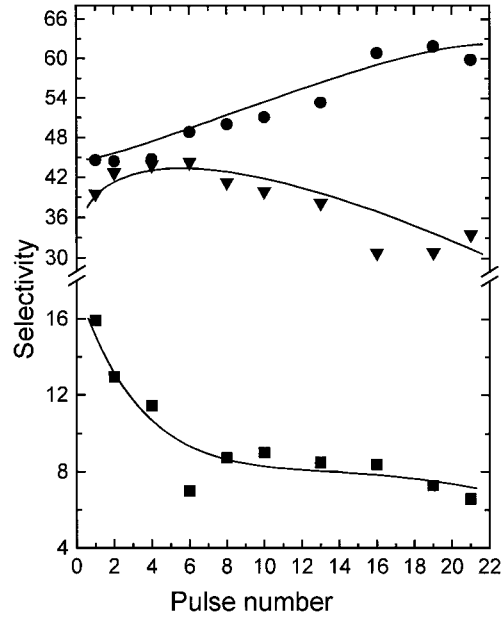

FIG. 12. Selectivity to butenes (●), butadiene (▼), and CO_x (■) during anaerobic experiments using butane pulses. Same conditions as in Fig. 11.

time, while the drop in selectivity to CO_x progressively slows down as the CO_x selectivity tends to very small values (ca. 6–7%).

DISCUSSION

The results of XRD and ^{51}V-NMR clearly show that the bulk of the VMgO catalysts was made up of mixed MgO (as the main phase) and $Mg_3V_2O_8$ orthovanadate. In both static and MAS NMR the 540 ppm peak related to the orthovanadate phase was narrower for the sample after testing under the most oxidizing conditions (O_2/But = 2). This suggests either an improved crystallization, in agreement with XRD results, or a decreasing amount of V^{4+} after reaction in an oxidizing atmosphere. Indeed, the presence of V^{4+}, which cannot be discarded in minor amount, could contribute to widening the V signal.

Regarding the surface analysis by XPS from Table 3, the high Mg/V atomic ratio (ca. 7) indicates that the prominent phase remains MgO, most likely coated with an amorphous V adlayer as demonstrated elsewhere (24). In addition, the fact that for all the samples the Mg/V atomic ratio from XPS was higher than the 6.66 value obtained by chemical analysis on the fresh sample can be understood by considering that part of the V is embedded in large vanadate crystals (up to 50 nm as deduced from XRD for the most highly crystallized sample); this would result in a depletion of the total amount of V available at the surface. Table 3 also illustrates several differences between fresh and used samples: Mg/O and V/O ratios increase for the used catalyst (which was expected given the partial reduction shown by TPR experiments). In addition, the Mg/V ratio tends to slightly decrease after use, which is in line with the above-mentioned reduction of the orthovanadate phase (Mg/V = 1.5) to a spinel-like phase (Mg/V = 0.5).

The XPS measurements indicate that a significant amount of V^{4+} is present in any of the samples (which indeed does not preclude the presence of V^{3+} species expected in a spinel-like reduced structure). The stability of the V^{5+}/V^{4+} ratio for samples contacted with different reaction atmospheres is somewhat surprising and perhaps could be due to an averaging surface oxidation during transportation of the reacted samples to the XPS chamber. This points out the limits of such an *ex situ* characterization technique. Instead, the ESR measurements confirm a clear increase in the V^{4+} content in parallel to the reducing character of the reaction atmosphere.

It seems to be generally accepted that the initial step of the reaction of butane with an oxidized VMgO catalyst is the abstraction of an H atom to give an adsorbed butyl group. The observation of the surface by infrared spectroscopy suggests that this adsorption could take place as a carboxylate, similar to the configuration proposed by Busca (20). The adsorbed species could then dehydrate to give an adsorbed olefin or even dehydrate/dehydrogenate to give a diolefin. The presence of both olefins and diolefins would contribute to the IR bands labeled as pseudo-graphitic or carboxylates/carbonaceous compounds. Olefins or diolefins could then desorb to give butene or butadiene, or remain adsorbed and undergo deep oxidation. The different mechanisms proposed for ODHB (2, 19–21) involve the generation of abundant surface OH groups as V–OH, and this has also been confirmed in this work, especially under oxygen-rich conditions.

Under oxygen-lean conditions the catalyst is found to be less active and more selective (Figs. 1 and 2). Because there is less active oxygen available at the surface, the reaction of the adsorbed species is slower which explains a lower activity. On the other hand, the lower concentration of nonselective oxygen increases the likelihood of the desorption of olefinic products as such against further oxidation to CO and CO_2.

The reactions that compete with oxidation, i.e., further dehydrogenation from butene to butadiene, are also favored by a lower rate of total oxidation. This indeed increases the yield to butene and butadiene, but also increases the production of low-reactivity, partially dehydrogenated carbonaceous species, which accumulate on the surface and lead to deactivation as evidenced from the DRIFT and TG measurements.

In spite of the formation of carbonaceous deposits, the catalyst used under oxygen-rich conditions was able to attain a relatively steady performance (Fig. 3) while keeping a significant fraction of its initial activity. In this case, a dynamic equilibrium between coke formation and gasification (by oxygen and steam) is established, leading to a stable activity. This is in sharp contrast with the usual observations in nonoxidative dehydrogenation of butane and butene (e.g., on Cr_2O_3/Al_2O_3 catalysts (49)), where the catalyst is often totally deactivated by coke in a short time.

It is interesting to note that the processes of formation of coke and butadiene on VMgO catalysts follow parallel patterns: the selectivity to butadiene decreases with time on stream (Figs. 3 and 9), and at the same time coke formation becomes slower (Fig. 10). Coke being a highly dehydrogenated carbonaceous species, it seems likely that the sites which are able to carry out a double dehydrogenation from butane to butadiene (butadiene is both a primary and secondary product (29)) might also be favorable for coke formation.

Because of the dynamic equilibrium between formation and gasification of carbonaceous deposits, part of the sites on the catalyst surface are free from coke, and these are responsible for the activity observed after the coke deposits reach a constant weight. With a higher oxygen/hydrocarbon ratio in the reacting environment the point of equilibrium is reached at a lower carbon coverage (0.17% instead

of 4.5% when the oxygen concentration increases to 8% from 4%), and the residual activity is considerably higher.

The changes in catalyst behavior under anaerobic conditions in Figs. 11 and 12 can be qualitatively explained by taking into account the characterization results already shown. Since the catalyst uses lattice oxygen for ODHB, a monotonic decrease in conversion is the expected behavior in the absence of gas-phase oxygen: as the catalyst becomes oxgygen-depleted on the surface, oxygen has to migrate from the bulk to the surface, which corresponds to a deep reduction of the system. Our characterization measurements show that such a deep reduction turns the VO_4^{3-} amorphous units (corresponding to the fully oxidized state) from the V^{5+} state into V^{4+} and most likely into the V^{3+} state (corresponding to a restructuration into a spinel-like structure). The reaction rate of ODHB at 500°C is high, which means that the process could be limited by the availability of oxygen at the surface, with a decrease in conversion when oxygen migration from the bulk is not able to match the surface reaction rates. It is also reasonable to expect the observed trend of monotonic increase for the selectivity to butenes: less available oxygen at the surface increases the chance of desorption before further oxidation of the butenes formed. In fact, the increase in selectivity as the catalyst becomes more reduced has been consistently reported in the literature (50, 51).

Another interesting feature is the conspicuous change of slope in the CO_x curve (Fig. 8) which strongly suggests the existence of two types of oxygen:

(i) One is readily reduced and reacts nonselectively. This kind of oxygen, accumulated on freshly activated catalyst (especially under oxygen-rich conditions, see Fig. 12) most likely consists of electrophilic adspecies such as O^- or O_2^-, which correspond to the first steps of gaseous oxygen activation (22, 23).

(ii) The second type of oxygen species is more difficult to reduce but gives mainly the desired oxidation products. This type of selective oxygen, which may be provided by the deep reduction of the catalyst, as above described, is associated with nucleophilic O^{2-} lattice oxygen. Its selective character may simply derive from its isolated position within the surface structure, at variance with the peroxidic or locally concentrated electrophilic species discussed above.

The selectivity to carbon oxides rapidly decreases as the first type of oxygen is consumed. Once the nonselective oxygen has been substantially eliminated a much smaller rate of decrease of the CO_x selectivity with pulse number is observed.

CONCLUSIONS

The surface of a VMgO catalyst during the oxidative dehydrogenation of butane is a highly dynamic system. The active and selective catalyst studied in this work presents V-coated magnesia and Mg orthovanadate as its main bulk phases during reaction, with a substantial amount of V^{4+}. However, the actual active surface is most likely an intermediate state between amorphous VO_4 units (V^{5+}) and crystallized spinel-like structure (V^{3+}) which could be achieved under highly oxygen-lean conditions. A certain degree of catalyst reduction is desirable for this reaction, because it increases the selectivity to dehydrogenation products by limiting the amount of oxygen available at the catalyst surface. This has been demonstrated in a variety of unsteady-state experiments using different techniques (DRIFT, step experiments with mass spectrometry, pulse experiments) which underlined the common feature that the selectivity increases continuously with catalyst reduction. A certain degree of catalyst reduction also helps to reduce the concentration of easily reducible oxygen species (probably adsorbed electrophilic oxygen), which reacts nonselectively.

However, the performance of the catalyst under highly oxygen-lean atmospheres is not stable. Catalyst deactivation is partly due to the fact that the catalyst is reduced, which renders it less active. Also, a certain contribution to deactivation from catalyst sintering cannot be ruled out, as suggested by the increase in crystal size observed with used catalysts. Nevertheless, the main cause for catalyst deactivation is the formation of coke, a process that occurs faster on reduced catalysts. As coke accumulates on the catalyst the rate of coke formation (and of butadiene production) decreases, until a point is reached where the rates of coke deposition and coke removal by oxidation and/or gasification become equal. From this point, the catalyst activity remains approximately constant. The level of this steady-state activity is higher as the oxygen/butane feed ratio increases (less coke deposits on the catalyst, less reduced catalyst), but the selectivity is lower.

ACKNOWLEDGMENTS

Financial support from DGICYT, Spain, project QUI98-0592 is gratefully acknowledged.

REFERENCES

1. Chaar, M. A., Patel, D., and Kung, H. H., *J. Catal.* **109**, 483 (1987).
2. Kung, H. H., *Adv. Catal.* **40**, 1 (1994).
3. Blasco, T., López-Nieto, J. M., Dejoz, A., and Vazquez, M. I., *J. Catal.* **157**, 271 (1995).
4. Martin-Aranda, R. M., Portela, M. F., Madeira, L. M., Freire, F., and Oliveira, M., *Appl. Catal. A* **127**, 201 (1995).
5. Vrieland, G. E., and Murchison, C. B., *Appl. Catal. A* **134**, 101 (1996).
6. Vrieland, G. E., Khazai, B., and Murchison, C. B., *Appl. Catal. A* **134**, 123 (1996).
7. Cavani, F., and Trifiró, F., "Catalysis," Vol. 11, p. 246. Royal Chem. Soc., London, 1994.
8. Bhattacharyya, D., Bej, S. K., and Rao, M. S., *Appl. Catal. A* **87**, 29 (1992).
9. Chaar, M. A., Patel, D., and Kung, H. H., *J. Catal.* **109**, 463 (1988).

10. Sam, D. S. H., Soenen, V., and Volta, J. C., *J. Catal.* **123**, 417 (1990).
11. Corma, A., López Nieto, J. M., and Paredes, N., *J. Catal.* **144**, 425 (1993).
12. Simakov, A. V., Sazonova, N. N., Ven'yaminov, S. A., Belomestnykh, I. P., Rozhdestvenskaya, N. N., and Isagulyants, G. V., *Kinet. Catal.* **30**, 598 (1987).
13. Chang, W. S., Chen, Y. Z., and Yang, B. L., *Appl. Catal. A* **124**, 221 (1995).
14. Oganowski, W., Hanuza, J., Drulis, H., Mi'sta, W. Y., and Macalik, L., *Appl. Catal. A* **136**, 143 (1996).
15. Patel, D., Kung, M. C., and Kung, H. H., *in* "Proceedings, 9th International Congress on Catalysis, Calgary, 1988" (M. J. Phillips and M. Ternan, Eds.), Vol. 4, p. 1554. Chem. Institute of Canada, Ottawa, 1988.
16. Kung, H. H., and Kung, M. C., *J. Catal.* **128**, 287 (1991).
17. Simakov, A. V., and Veniaminov, S. A., *React. Kinet. Catal. Lett.* **1**, 67 (1985).
18. Le Bars, J., Vedrine, J. C., and Auroux, A., *Appl. Catal. A* **88**, 179 (1992).
19. Blasco, T., and López Nieto, J. M., *Appl. Catal. A* **157**, 17 (1997).
20. Busca, G., *Catal. Today* **27**, 457 (1996).
21. López Nieto, J. M., Concepción, P., Dejoz, A., Knözinger, H., Melo, F., and Vazquez, I., *J. Catal.* **189**, 147 (2000).
22. Pantazidis, A., Auroux, A., Herrmann, J.-M., and Mirodatos, C., *Catal. Today* **32**, 81 (1996).
23. Pantazidis, A., and Mirodatos, C., *in* "Heterogeneous Hydrocarbon Oxidation" (B. K. Warren and S. T. Oyama, Eds.), ACS Symposium Series, Vol. 638, p. 207. Am. Chem. Soc., Washington, DC, 1996.
24. Pantazidis, A., Burrows, A., Kiely, C. J., and Mirodatos, C., *J. Catal.* **177**, 325 (1998).
25. Schuurman, Y., Décamp, T., Jalibert, J. C., and Mirodatos, C., *in* "Reaction Kinetics and the Development of Catalytic Processes" (G. F. Froment and K. C. Waugh, Eds.), Studies in Surface Science and Catalysis, Vol. 122, p. 133. Elsevier, Amsterdam, 1999.
26. Soler, J., López-Nieto, J. M., Herguido, J., Menéndez, M., and Santamaría, J., *Catal. Lett.* **50**, 25 (1998).
27. Soler, J., López-Nieto, J. M., Herguido, J., Menéndez, M., and Santamaría, J., *Ind. Eng. Chem. Res.* **38**, 90 (1999).
28. Dejoz, A., López Nieto, J. M., Melo, F., and Vazquez, I., *Ind. Eng. Chem. Res.* **36**, 2588 (1997).
29. Téllez, C., Menéndez, M., and Santamaría, J., *J. Catal.* **183**, 210 (1999).
30. Creaser, D., and Anderson, B., *Appl. Catal. A* **141**, 131 (1996).
31. Michaels, J. N., Stern, D. L., and Grasselli, R. K., *Catal. Lett.* **42**, 139 (1996).
32. Stern, D. L., and Grasselli, R. K., *J. Catal.* **167**, 560 (1997).
33. Pantazidis, A., Ph.D. thesis, Lyon, 1996.
34. Jalibert, J. C., Ph.D. thesis, Lyon, 1999.
35. Boisdron, N., Monnier, A., Jalowleckl-Duhamel, L., and Barbaux, Y., *J. Chem. Soc., Faraday Trans.* **91**, 2899 (1995).
36. Zanthoff, H. W., Buchholz, S. A., Pantazidis, A., and Mirodatos, C., *Chem. Eng. Sci.* **54**, 4397 (1999).
37. Mamedov, E. A., and Cortés Corberán, V., *Appl. Catal. A* **127**, 1 (1995).
38. Corma, A., López Nieto, J. M., Paredes, N., Dejoz, A., and Vazquez, M. I., *in* "New Developments in Selective Oxidation II" (V. Cortés Corberán and S. Vic Bellón, Eds.), Studies in Surface Science and Catalysis, Vol. 82, p. 113. Elsevier, Amsterdam, 1994.
39. Burrows, A., Kiely, C. J., Perregaard, J., Højlund-Nielsen, P. E., Vorbeck, G., Calvino, J. J., and Lopez-Cartes, C., *Catal. Lett.* **57**, 121.
40. Lapina, O. B., Simakov, A. V., Mastikhin, V. M., Veniaminov, S. A., and Shubin, A. A., *J. Mol. Catal.* **50**, 55 (1989).
41. Gao, X., Ruiz, P., Xin, Q., Guo, X., and Delmon, B., *J. Catal.* **148**, 56 (1994).
42. Gao, X., Ruiz, P., Xin, Q., Guo, X., and Delmon, B., *Catal. Lett.* **23**, 321 (1994).
43. Socrates, G., *in* "Infrared Characteristic Group Frecuenies," 2nd Ed. Wiley, Chicester, 1980.
44. Ramis, G., Busca, G., and Lorenzelli, V., *J. Chem. Soc., Faraday Trans.* **90**, 1293 (1994).
45. Finocchio, E., Ramis, G., Busca, G., Lorenzelli, V., and Willey, R. J., *Catal. Today* **28**, 381 (1996).
46. Ibarra, J. V., Royo, C., Monzón, A., and Santamaría, J., *Vib. Spectrosc.* **9**, 191 (1995).
47. Pantazidis, A., and Mirodatos, C., *in* "Proceedings, 11th International Congress on Catalysis, Boltimore, 1996" (J. W. Hightower, W. N. Delgass, E. Iglesia, and A. T. Bell, Eds.), p. 1029. Elsevier, Amsterdam, 1996.
48. Dadyburjor, D. B., and Liu, Z., *Chem Eng. Sci.* **47**, 645 (1992).
49. Peña, J. A., Monzón, A., and Santamaría, J., *J. Catal.* **142**, 59 (1993).
50. Andersen, P. J., and Kung, H. H., *in* "Proceedings, 10th International Congress on Catalysis, Budapest, 1992" (L. Guczi, F. Solymosi, and P. Tetonyi, Eds.), Vol. A, p. 205. Elsevier, Amsterdam, 1993.
51. Kung, H. H., and Kung, M. C., *Appl. Catal. A* **157**, 105 (1997).